Mustansiriyah Journal of Pure and Applied Sciences

www.MJPAS.com

Degradation of Organically Polluted Water by Photocatalysis of SnO_2:CuO Nanocomposite Under the Influence of Sunlight

R.A. Al-Mousawi[1,2], A.A. Saeed[3], M.F. Al-Kadhemy[4]and K.N. Abbas[5]

[1,3,4,5] Department of Physics Science, College of Science, Mustansiriyah University, Baghdad, Iraq
([1]rawasiaiad@uomustansiriyah.edu.iq,[3]dr.asrar@uomustansiriyah.edu.iq,
[4]dr.mahasin@uomustansiriyah.edu.iq,[5]khnaa@uomustansiriyah.edu.iq)
[2]Department of Physics Science, College of Science, Nahrairn University, Baghdad, Iraq.

A B S T R A C T

Reactive dyes pose a major risk to the environment and human health when they contaminate water .In this study we prepared highly efficient a synthesis of SnO_2:CuO nanocomposite with two different concentrations by environmentally friendly which is hydrothermal method. The technique of X-ray diffraction was used to examine the structural properties of the materials, The FE-SEM technology was utilized to explore and evaluate the surface morphology, FTIR and UV–visible spectrophotometer. The results reveal from XRD that the crystal structure of samples exhibits two phases comprising SnO_2 structure that possesses tetragonal rutile, tetragonal cell of metallic Sn, and monoclinic-phase of CuO. FESEM images detect that the change of precursor concentration in the range of (0.1-0.05 M) influence the shape of the nanocomposite and has an amazing effect on the diameter size as-grown particles in the range of (53.8-22.73) nm and photocatalysis. The FTIR spectra's presence of vibrational bands corresponding to CuO and SnO_2 confirms that these materials exist in the nanostructure, showing that the binaries of metallic oxides have been integrated successfully. In UV-Vis., absorption increase with thickness layer. With rising thickness layer, the energy gap dropped from (2.05 to 1.98) eV. Using Methylene blue as a model pollutant, the photodegradation efficiency of SnO_2:CuO nanocomposite was investigated. SnO_2:CuO (95% and 92% at 135 min.) The hydrothermal approach with two different concentrations supports the photocatalytic activity observed in this work to remove methylene blue, and the result is to preserve the aquatic environment as much as possible.

Keywords: *SnO_2:CuO nanocomposite, photocatalytic, Sunlight, Methylene blue (MB), Hydrothermal method, Structural morphological, Optical properties*.

1. Introduction

The most dangerous environmental contamination is being produced by the rapid industrialization and civilization process. One of the main issues facing eco-friendly environments is water contamination [1]. In addition to having detrimental effects on health, water pollution has altered the way of life for aquatic organisms [2]. Additionally, the number of premature fatalities rose daily as a result of water pollution [3]. Wastes from the textile, food, paint, and leather industries (organic pollutants) are difficult to recycle or purify because they can easily combine with water resources [4]. The development of quick, highly effective, and inexpensive physical, chemical, and biological degrading methods is of great interest to research communities. Due to its simplicity, environmental friendliness, and ability to degrade organic pollutants without producing any secondary products, solar-driven semiconductor-based photocatalysis technology has drawn the most attention among them [5, 6]. For the photocatalysts procedure, many semiconductor materials were utilized, such as metal oxide [7-9], Sulfide of a transition metal [10, 11], carbon-based substances [12, 13], as well as MOFs (metal-organic frameworks). Metal oxide is one of those that has received the most attention in the photocatalytic area because of the material's strong chemical stability, low danger composition, wide bandgap, and high exaction binding energy. The metal oxide in the majority of semiconductors only absorbs UV light., this limits their applicability [14]. In addition to covering the visible and UV bands, using two metal oxides together improved the photocatalytic characteristics. The wide bandgaps (3.7 eV) and high exciton binding energies (60 m eV) of these materials, systems for electronics, optics, and photonics are increasingly using metal oxide nanostructures. [15, 16]. The formation of the (n-p) junction between SnO_2:CuO heterojunction among them enhanced the photocatalytic characteristics because of their wide bandgap, non-toxic composition, strong photosensitivity, and low recombination rate. CuO (1.5 eV) is a p-type semiconductor, and SnO_2 (3.7 eV) is a broad bandgap n-type semiconductor. When CuO acts as a sink in an n-p heterojunction, the photogenerated electron-hole pair migrate in the opposite direction, accumulate in the valence band of SnO_2, and efficiently pairs of electrons and holes recombine less frequently. This helps to separate the electron-hole pair (reduced recombination). The high migration of electrons in the opposite direction combined with minimal recombination would increase the photocatalytic property of the SnO_2:CuO heterostructure, heterostructure of SnO_2 with CuO [17, 18]. Hydrothermal approach used in this study to create the SnO_2:CuO heterostructure photocatalyst is of special interest because it is economical and environmentally benign, with growth temperatures as low as 90 °C [19]. The hydrothermal method involves heating and pressurizing an aqueous solution to operate as a reaction system in a particular closed reaction vessel in order to provide a high-temperature, high-pressure reaction environment [20].

The aim of the research is to remove organic pollutants from the water by photocatalysis and to preserve the environment by using the available and free sunlight by choosing a method for preparing low-temperature materials that are low-cost and within the range of environment-friendly and use of catalytic materials with toxicity is very little or negligible and high response to photocatalytic process.

2.Experimental

2.1Materials

the kinds of components, molecular weight, manufacturer, and purity used in manufacturing were (Tin chloride dehydrate) Tin (II) chloride [SnCl2.2H2O , Sigma-Aldrich, purity 98%, Wt. 241.6], copper (II) nitrate trihydrate [NO32.3H2O, HIMEDIA-India, extra pure 99.5%, Wt. 225.6], ethanol (C2H5OH, 100% purity , Hayman, UK, Wt. 46.07), glass substrate [China's Yingke Optical Products Co., Ltd]. methylene blue dye [C16H18N3ClS, Sigma-Aldrich,99.9%, Wt.319.85] was utilized to evaluate the performance of a photocatalytic process. Distilled water (DW) was used for the experiment.

2.3 Synthesis of SnO_2:CuO nanocomposite

In this research, by modifying the hydrothermal growth conditions, two samples of (SnO_2:CuO) nanocomposite where it has been prepared by this method and is considered one of the methods of low cost, easier to manage composition, deposition over a larger area, and operates at lower temperatures. With tin chloride SnCl2.2H2O as a tin source in addition, a copper source is copper nitrate, Cu (NO3)2.3H2O., as shown in Fig (1). The specific synthesis steps were as follows: First, by melting (2.256 g/mol) of SnCl2.2H2O in 100 ml of deionized water (DW), the SnO_2 precursor solution was created, it was swirled with a stirrer that was magnetized for ten minutes at a temperature of 50 °C. Also, (2.416 g/mol) of Cu (NO3)2.3H2O was dissolved in 100 ml of DW to obtain the CuO precursor solution. After mixing and stirring the two precursor solutions for 15 minutes at room temperature, NaOH had been added to the mixture to bring the pH value to (10). The combination that resulted was poured into a glass autoclave (200 ml) and subjected to heating treatment at 130 °C for 4 hour). The finished product powder was centrifuged at a speed of 2000 r/min., cleaned four times with deionized water and once with ethanol, and dried at 70 °C for an hour. The final product was created by placing the product powder into a tube furnace and annealing it at 50 °C for one hour. We repeat all the previous steps by changing the concentrations of SnCl2.2H2O and Cu (NO3)2.3H2O as shown in.

Table 1. concentrations of SnCl2.2H2O and Cu (NO3)2.3H2O

Sample	Concentration SnCl2.2H2O g/mol	Concentration Cu (NO3)2.3H2O g/mol
S1	0.1	0.1
S2	0.05	0.05

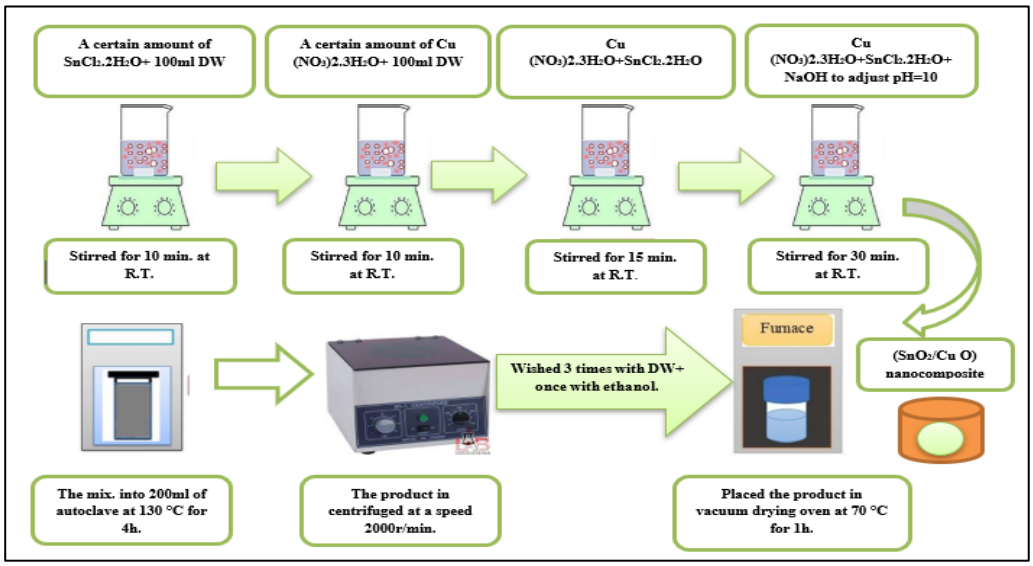

Figure1. Schematic illustration the preparation steps of SnO2/CuO nanocomposite by hydrothermal method.

2.4 Study of photocatalysis

The degradation of organic contaminants under visible light was used to evaluate the photocatalytic capabilities of the (SnO_2:CuO) nanocomposite. 1 liter of Distilled water (DI) water containing 10 mg/ml of methylene blue dye was stirred for 15 minutes. The mixture was then combined with 5 mL of the heterogeneous catalyst SnO_2:CuO (S1 and S2) for 30 minutes in the dark to allow impurities to build up on the film. The usual contamination was then made to come into contact with the catalyst using sunlight. Organic matter Methylene blue (MB) was exposed to the contaminated solution for 45 minutes before the UV-vis absorption spectra was examined. The photocatalytic efficacy (P) is determined by Eq. (1) [21]

$$P = \frac{Co - Ct}{Co} * 100\% \quad (1)$$

The starting dye concentration is C_o ($mg1^{-1}$) and the final concentration is C_t ($mg1^{-1}$) after a predetermined amount of time. The (MB) absorption spectra in a solution containing 10 mL of dye could be recognized at 663 nm.

Several analysis instruments were used to characterize the prepared SnO_2:CuO nanocomposite samples. The structural characteristics were examined using X-ray diffraction (XRD). "Shimadzu XRD-6000" was used to obtain (2Θ) scans at a Bragg range of (20◦-80◦), FTIR (Fourier-transform infrared spectroscopy) is done using (BIOTECH ENGINEERING MANAGEMENT) to study the compositional properties. By using field emission-scanning electron microscopy (FESEM; Hitachi-S 4160-Japan), images of the surface morphology and cross-section of four materials were obtained. A UV-Vis spectrometer of the T70/T80 Series UV/Vis type was used to investigate the optical qualities represented by absorption spectra in the wavelength range of 200-900 nm.

3.Structural Analysis (XRD)

The hydrothermal process for making SnO_2:CuO nanocomposite at various concentrations for growth period of 4 h, temperature of 130 C, and pH = 10 is shown in Fig. (2). The placements of samples' XRD peaks can easily be correlated with SnO_2's tetragonal structure (JCPDS 21-1250) [22], monoclinic-phase of CuO (JCPDS 80–1268) [23] and Sn (JCPDS 86-2265) [24]. These XRD peaks of the SnO_2 structure corresponded to the (110), (132), (041), (223), (400), (204), (210), (211), (220), (002) and (310) miller indices. While the XRD diffraction peaks of tetragonal Sn agreed with the (110) miller indices. Lastly the XRD diffraction peaks of the CuO agreed with the (002), (200), (-112), (-202), (202), (-311) and (113) miller indices. This proves that SnO_2 and CuO are separate phases that coexist in the doped thin film. [25]. The average crystal size of the resulting SnO_2:CuO is around (45-54) nm, obtained using Scherrer's Eq. (2) [26] and in the table (2).

$$D = \frac{0.9\lambda}{\beta\, Cos\theta} \qquad (2)$$

where D is the size of the crystal and (λ) is the wavelength of the light, which is 1.5408 Å, (β) represents the peak's whole width half maximum in radians, while (Θ) denotes the Bragg angle.

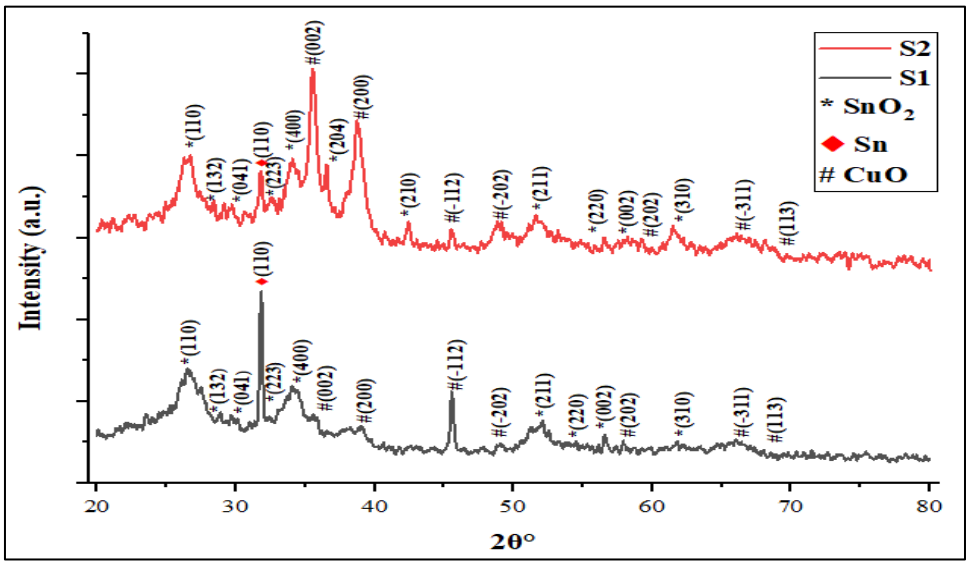

Figure 2. XRD patterns of as-prepared SnO_2:CuO nanocomposite synthesis by hydrothermal method at different concentration for growth time 4 h, growth temperature 130 C and pH = 10

When both SnO_2 and CuO are present, a composite has formed. The broad appearance of the peaks in samples S1 and S2 indicates that the small-sized nanocrystalline SnO_2:CuO is formed. Sharp diffraction peaks reveal the crystalline nature of all NPs, whereas extra peaks are seen in the XRD spectrum of samples because of the Sn metal powder at the angle 31.84, displays sharper and more intensified Sn peaks, indicating an increase in the Sn particle size, that results agree with studies [27-29]. Due to the formation of crystallites and the enhancement of crystallization, the SnO_2:CuO nanocomposite's diffraction peak strength in samples S1 and S2 clearly increases, while the peak's width gradually decreases. The SnO_2 exhibits five main peaks, while the CuO powder displays four distinct major peaks. It is significant to notice that the XRD pattern of the SnO_2:CuO nanocomposite, which corresponds to the (0 0 2) plane of CuO, shows a modest peak at about $2\Theta = 35.88$ in S1 with a peak intensity that is larger in S2, and the most intense peak, which was associated with CuO in sample S2 and Sn in sample S1, at diffraction angles 38.79 and 31.84, respectively, which demonstrates the favored direction for the formation of nanocrystals.

The presence of secondary metal in the produced nanostructure is clearly indicated by the broadness in the XRD pattern, that agree with [30]. The CuO samples served as dopants in the SnO_2 structure, according to the x-ray diffraction patterns shown in Fig. 1 and table (2), since the diffraction peaks of SnO_2 were more intense than those of CuO, which was caused by their dissociation constant [25]. Since a distinct peak (Sn) was seen, it cannot be said that the thin film that was created simply consisted of SnO_2 and CuO crystal phases. SnO_2:CuO nanocomposites' pattern shows a peak at

position (110) that is greater in 2 value and is caused by an increase in oxygen vacancies [31], As a result of flaws or the presence of secondary species in the material, residual stresses or lattice contraction may be caused (Sn). Since it has been widely reported that defects like oxygen vacancies and oxygen interstitials, in addition to other factors like phase purity, nature of dopant, method of synthesis, shape, particle size, morphology, and surface area, are primarily responsible for light-mediated activity such as photocatalysis, the presence of such defects in nanocomposite is encouraging [32].

Table 2. XRD analysis results of SnO_2:CuO nanocomposite synthesis by hydrothermal method

Material	Concentration	(h k l)	D (nm)	d (A)	FWHM (Deg.)
SnO_2+CuO (Nanocomposite)	0.1+ 0.1 M	110	56.69	3.36	0.144
		132	25.61	3.14	0.32
		041	68.52	3.00	0.12
		110	45.89	2.80	0.180
		Sn	**Sn**	**Sn**	**Sn**
		223	13.21	2.74	0.6267
		400	21.70	2.64	0.3828
		204	15.50	2.45	0.54
		210	19.82	2.13	0.43
		211	36.82	1.76	0.24
		220	110.70	1.68	0.0807
		002	47.58	1.62	0.189
		310	77.20	1.49	0.12
			average crystal size = 45 nm		
SnO_2+CuO (Nanocomposite)	0.05 + 0.05 M	002	65.26	2.50	0.128
		200	70.22	2.31	0.12
		-112	47.21	1.98	0.182
		-202	58.19	1.86	0.15
		202	43.67	1.59	0.208
		-311	75.22	1.41	0.126
		113	17.058	1.38	0.56
			average crystal size =56 nm		

4.Morphology Analysis

Using FE-SEM images, the surface and cross-section of SnO_2:CuO nanocomposites were further described and investigated in response two different precursor concentration. These samples were created using the hydrothermal process over the course of four hours with a heating treatment at 130 °C and a pH of 10. The creation of the dense nanoparticle aggregation of the SnO_2:CuO nanocomposite (S1) by

applying a precursor mixture consisting of (0.1 M of SnO_2 + 0.1 M of CuO) is shown in FE-SEM images in Fig. 3-a-b The average particles (53.8) nm in size as seen in fig. (3-a).

When the pH is 10 and the incubation time is 4 hours, there is a greater development of NPs that are clustered, homogenous, and clearly semi-spherical in shape. The stability of cluster dispersion under given circumstances Increased reaction time may have contributed to this outcome, and as reaction time increases, so does the crystallization of smaller particles, which involved the nucleation and development of smaller particles from SnO_2:CuO nuclei. The surfaces of both SnO_2:CuO synthetic materials can be seen in the FE-SEM pictures to be densely packed with uniform nanospheres. The cross-section of the sample (S1) as it was created was calculated to be (1.64μm), which is corroborated by Fig. (3-b).

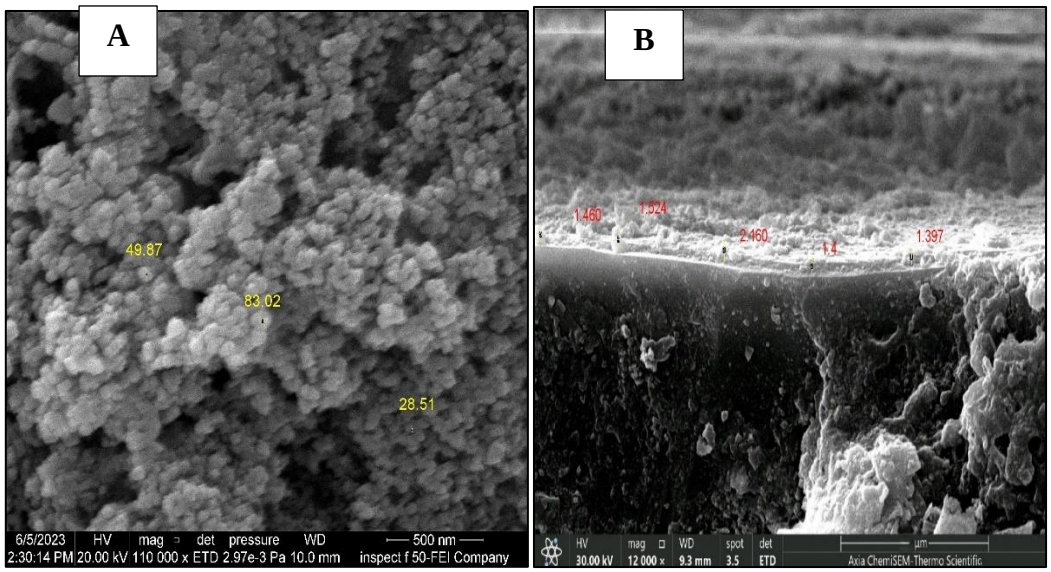

Figure 3-a-b. FE-SEM image and cross-section of SnO_2:CuO nanocomposite as-prepared by a hydrothermal method under pH=10, at 130 °C and growth time 4 h

Fig. 4-a-b explains surface image and the cross-section of SnO_2:CuO nanocomposite (S2) prepared at concentrations (0.05 M of SnO_2 + 0.05 M of CuO). The morphology displays the particles' homogeneous, dense, and packed packaging. This indicates the possibility of controlling the size of NPs by the pH, reaction time, and concentration. The nanoparticle in these conditions is that the particles appear in the form of very small, almost spherical clusters, and the particles are grouped in a compact manner because of agglomeration. The high surface interaction between nanoparticles, which have a large specific surface area and high surface energy, or which may have been brought on by thermal stress, is what causes the agglomeration of nanoparticles [25]. The average particles (22.73) nm in size as seen in fig. (4-a).

It is noted from the fig.(4-b) the cross-section was calculated to be (4.1μm), that the prepared nanomaterials are seen at homogeneous in an organized and dense

manner resembling clouds i.e., densely packed homogeneous nanospheres are across the entire surface of synthesized materials. Finally, we conclude that the lower the concentration, the lower the NPs.

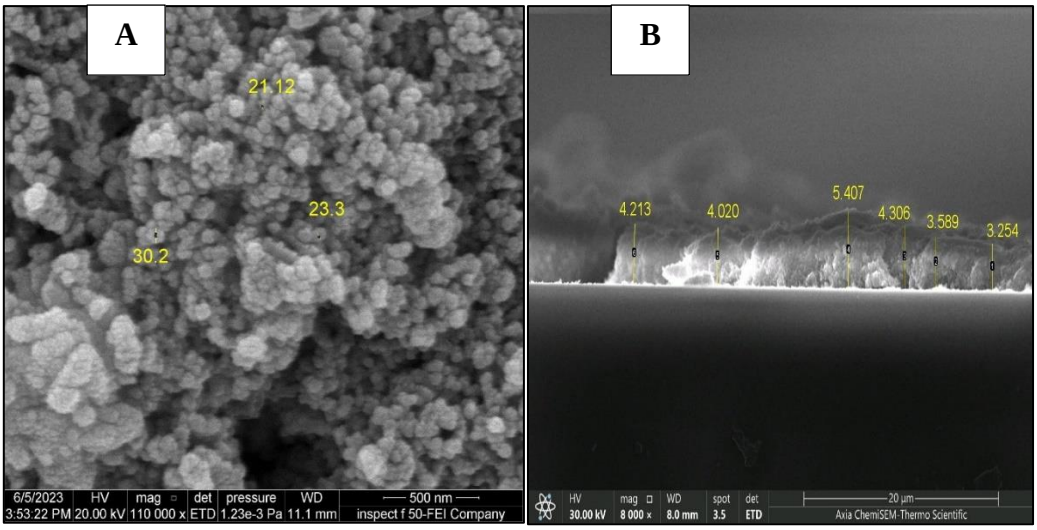

Figure 4-a-b. FE-SEM image and cross-section of SnO_2:CuO nanocomposite as-prepared by a hydrothermal method under pH=10, at 130 $^{\circ}$C and growth time 4 h

Fig. 5-a-b shows the FTIR spectra of the two prepared samples. The band at (668.86, 654.98 and 669.27) cm^{-1} for S1 and S2 equally correlates to the asymmetric stretching vibrational mode of the Sn-O, indicating that no additional phase of copper was present in the synthesized product. The band at (461.31, 493.30, and 419.13) cm^{-1} for two samples represents the bending vibrational modes of Cu-O, that agree with studied [25]. As a result of a condensation process between Sn-OH groups during to generate Sn-O-Sn, the peaks grew stronger and weaker, respectively [33]. In the metal to oxide bond, the formation of the O-Sn-O bridging link at (720.09) cm^{-1} for S2 corresponds to the production of symmetric stretching vibrations. It was determined that the Sn-OH stretching bond was responsible for the peak in S1 at (914.20) cm^{-1}. The absorption bands at (2272.10-2360.69) cm^{-1} are mostly caused by chemisorbed and/or physiosorbed molecules of H_2O and CO_2 on the surface of nanostructured hierarchical copper oxide crystals. Peak (1362.53) cm^{-1} refer to CH_2 bending and (Cu-OH) stretching. There are no peaks between 1500 cm^{-1} in S2 because of the oxygen's sheer vibrational stretching. [34], only in S1 appear the peak (1593.75) cm^{-1} which refers to (C=C) stretching.

A

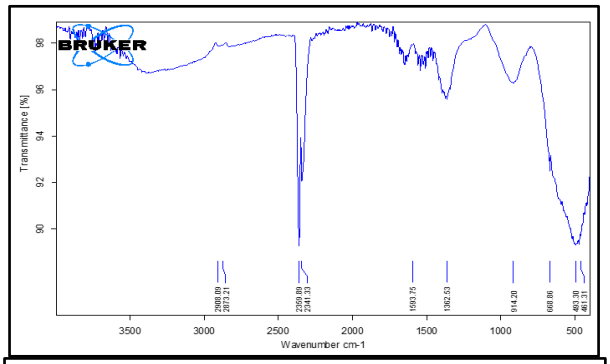

B

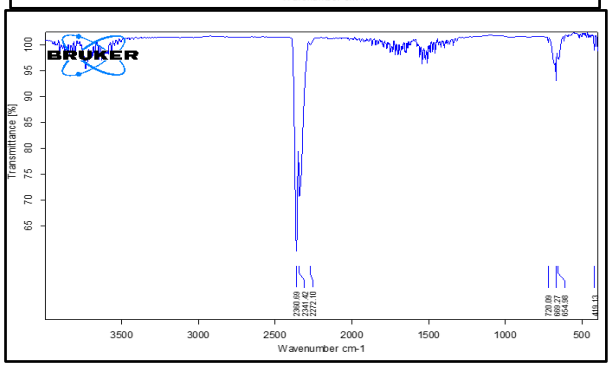

Figure 5-a-b. Showed the FTIR spectra of SnO_2:CuO dependent different concentrations of precursor solutions at pH = 10, T= 130 C and growth time 4 h

5.Optical Properties

A UV-Vis. spectrophotometer usual to it examine the optical absorption spectra of SnO_2:CuO nanocomposite samples in the 200-900 nm region, as shown in Fig. (6-a). The peaks of S1 are (360) nm shown at a with concentration of (0.1 SnO_2 + 0.1 CuO) mol. While the peaks of S2 is (370) nm for concentration (0.05 SnO_2 + 0.05CuO) mol.

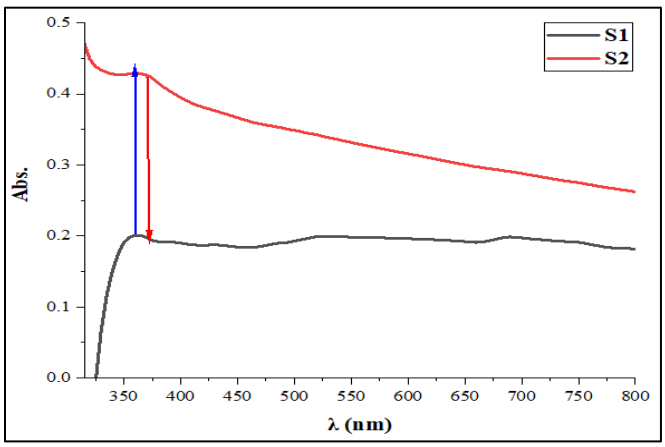

Figure 6-a. UV-Vis spectra of SnO_2:CuO dependent different concentrations of precursor solutions at pH = 10, T= 130 C and growth time 4 h

The size and structure of the NPs, the surface roughness, and impurities are some of the variables that affect absorption [35]. From the above fig. (6-a) and table (4) The absorption peak intensity increases with increasing thickness layer, and time reaction. The strong interfacial connection between NPs, where the homogeneity and regularity of nanomaterials occur, or so-called crystalline regeneration, is one of the causes of the increase in absorbance with layer thickness; this led to higher absorption and decreased transmittance, Since the film packing density rises with increasing film thickness, the relationship between increasing film thickness and light absorption can be explained by an increase in the effective optical path length [36]. The main cause of the blue-shift seen in S1 is the quantum size effect on the reduced size of SnO_2:CuO nanoparticles. While in sample S2 there is a movement towards the red due to flaws, there may be significant variation on the properties of nanocrystalline materials observed compared to bulk qualities when the particle size decreases from bulk to nano.

The energy band gap of SnO_2:CuO nanocomposite was estimated by plotting the square of $(\alpha h\upsilon)^2$ versus photon energy ($h\upsilon$). The extrapolation of the straight line to $(\alpha h\upsilon)^2$ gives the value of the energy gap. The optical band gap of the SnO_2:CuO nanocomposite varied from 2.05 to 1.98 eV. $(hv)^2$ $(ev/cm)^{2,}$ as shown in fig. (6-b) and table (3).

Moreover, the following equation (3) can be used to calculate the energy band gap [37]:

$$\alpha h\upsilon = B(h\upsilon - Eg)^x \quad (3)$$

Where Eg: is the optical energy band gap; h: is photon energy; B: is a constant, and x: is constant, the allowed and forbidden direct transitions are (1/2, 3/2), respectively, while the allowed and forbidden indirect transitions are (2, 3), respectively.

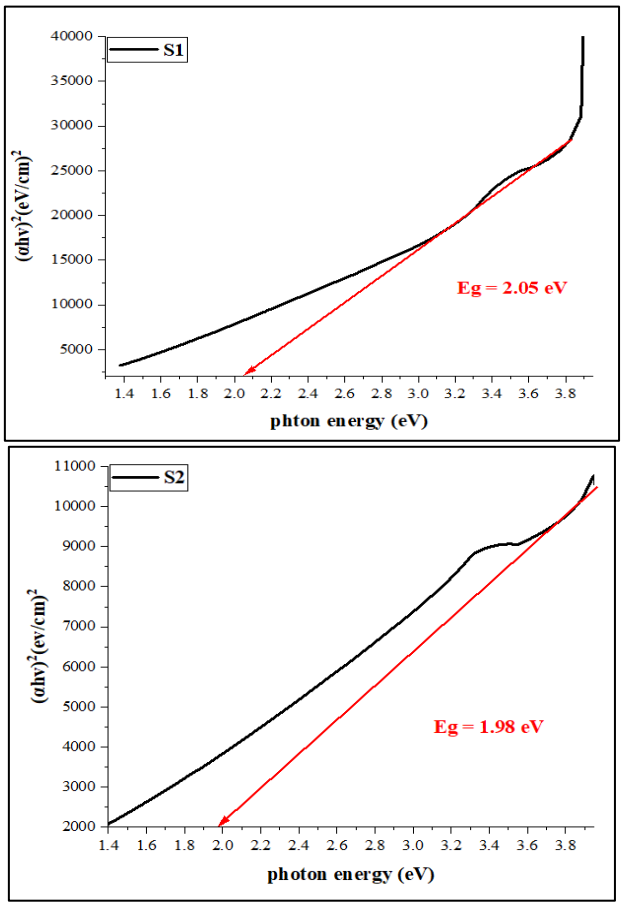

Figure 6-b. Energy gap of SnO_2/CuO dependent different concentrations of precursor solutions at pH =10, T= 130 ̊C and growth time 4 h

Depending on the film crystal structure, the atoms' arrangement, and their distribution inside the crystal lattice, the energy band gap (Eg) values [38]. FESEM confirms that the band gap shrunk because of the creation of nano-sized particles. The Eg continually decreases with layer thickness, mostly because of quantum confinement in the SnO_2:CuO nanocomposite. As a result, the existence of unstructured defects that raise the density of localized states in the band gap and subsequently lower the energy can be blamed for the decrease in optical band gap with increasing film thickness layer [39]. The minor shift in the energy gap may be due to strain created in SnO_2:CuO that causes quantum confinement in the heterostructures or variations in crystalline size across the sample [40, 41].

Table 3. Optical measurement of SnO_2:CuO dependent different concentrations of precursor solutions at pH = 10, T= 130 C and growth time 4 h

Sample	Concentration condition	Thickness layer (cross-section) (cm)	Energy gap (e.v)
S1	0.1 (SnO_2) +0.1 (CuO)	0.000164	2.05
S2	0.05 (SnO_2) +0.05 (CuO)	0.000413	1.98

6.Photocatalytic process

Samples obtained through a hydrothermal process to demonstrate their photocatalytic activity; nanocomposite was employed to breakdown the bonds of methylene blue in the presence of sunshine. Figure (7-a-d) illustrates the examination of the photocatalytic characteristics of the SnO_2:CuO nanocomposite, exhibits the UV absorption spectra of the model pollutant. The degradation rate of methylene blue was calculated using the computed proportion of SnO_2:CuO and the UV-vis absorption spectra, which was determined to be (92.57%, 90.85%, 83.42%) in S1 and (95.08%, 94.28%, 79.54%) in S2 respectively, as can be seen in Fig. (7-a1-a2). It is evident that as exposure time lengthens, the absorption peaks of the (MB) dye gradually fade away. Approximately (95%) of the MB may be dissolved in 135 minutes. Figure (7-b) depicts the time-dependent photodegradation of methylene blue, which exhibits an increase in deterioration when exposed to sunlight. Additionally, after 135 minutes, as indicated in fig. (7-c), the disintegration of methylene blue by SnO_2:CuO nanocomposite generated by hydrothermal is high. The concentration-time equation may be used to determine the pseudo-first-order rate constant k (min^{-1}) from the slope line of fig. (7-d) and Eq. (4) [42]:

$$Ln.\ (Co/C) = kt. \quad (4)$$

where k is the first-order rate constant, C_0 is the initial concentration of the MB dye and C is the reaction concentration at time t. It is discovered that the by hydrothermally synthesized heterojunction's values for (k) of methylene blue are (0.019 min^{-1}) for S1, while (0.022 min^{-1}) for S2. Thus, the photodegradation efficiency of the SnO2/CuO heterojunction prepared by hydrothermal is high. The ideal SnO_2:CuO concentration for sample (S2) raised the trap state in the nanocomposite and decreased the rate at which electrons "e-" and holes "h+" recombined [43].

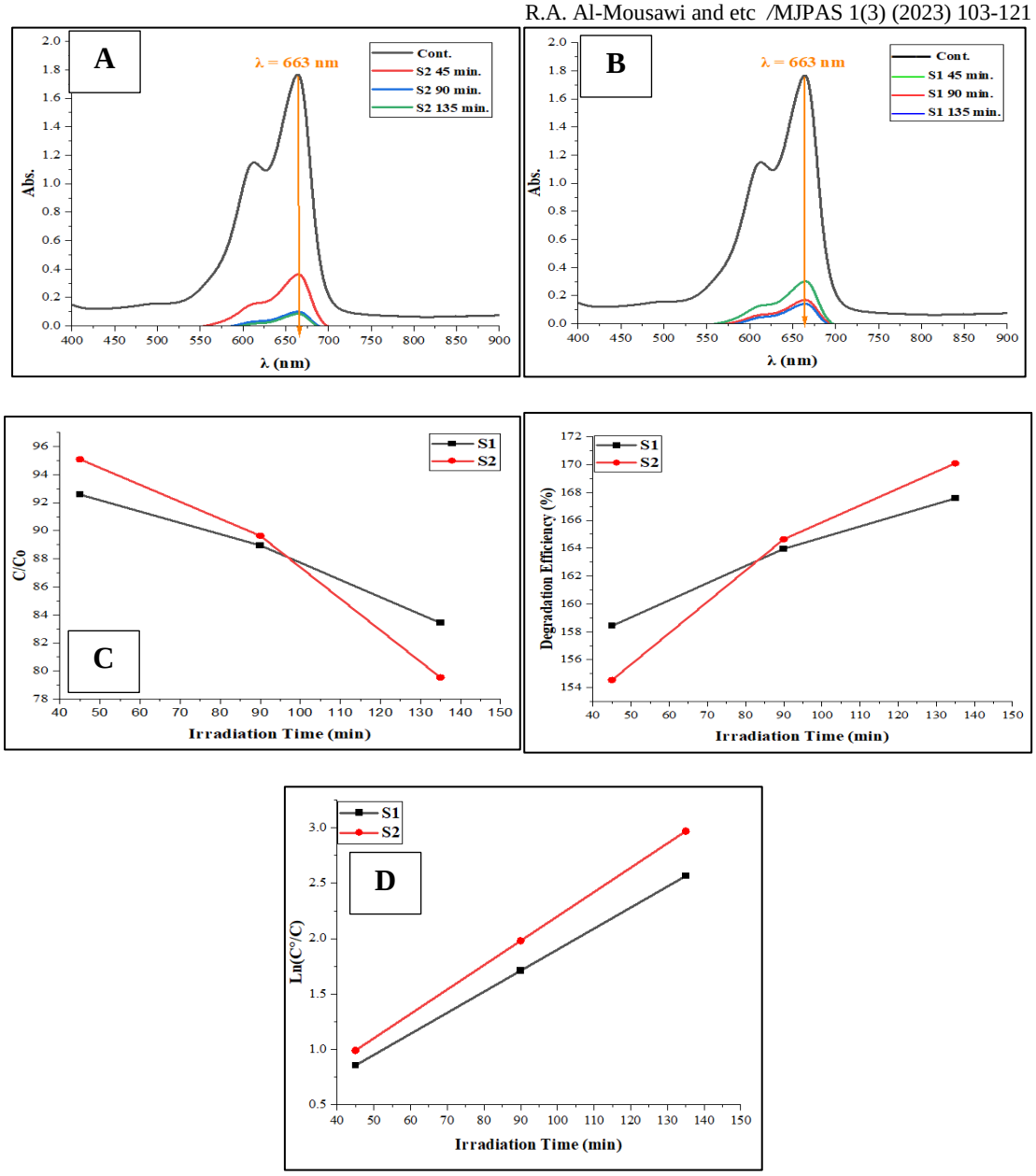

Figure 7-a-d. (a) The UV-vis absorption spectra were used to calculate the dye's degradation rate, (b) The time-dependent photodegradation of dye, (c) the degradation efficiency of dye by the (SnO_2:CuO) and (d) first-order kinetics of dye below the sun light.

It is well known that two key elements affecting the photocatalytic activity are the crystallization and surface area of the photocatalyst. The crystallites grow larger as crystallization progresses [44]. The results show that the SnO_2:CuO photocatalyst in S2 (SnO_2 to CuO molar ratio is 0.05:0.05) at 130°C for 135 min obtains the highest photocatalytic activity with MB solution. This is likely due to the samples' excellent crystallization and high surface area. However, due to the reduction in surface area or the occurrence of some sintering, the photocatalytic activity of the photocatalyst in S1a somewhat decreased at the concentration (0.1 SnO_2+0.1 CuO) [45]. The bandgap values of the produced samples, which range from 2.05 to 1.98 eV, support the

semiconducting nature of SnO_2:CuO nanostructures. Excitation is the process by which electrons in the valence band that are exposed to light tend to absorb photon energy and move to the higher energy conduction band (CB). These conduction band electrons generate the highly reactive Super Oxide Anion (O_2*) when they interact with the ambient oxygen. Due to their strong reducing nature, these Super Oxide Anion breakdown the organic dye (MB) when they come into contact with it, producing non-toxic byproducts like CO_2 and H_2O.

Photocatalyst + hυ ⟶ (CB) e^- + (VB) h^+

Atmospheric O_2 + (CB) e^- ⟶ Super Oxide Anion (O_2*)

H_2O + (VB) h^+ ⟶ H^+ + Hydroxyl radical (OH•)

OH• / O_2* + Organic dye (Methylene blue)

Similar to how electrons that have moved to a higher energy level after absorbing extra energy leave holes in the valence band (VB), the hydroxyl radical (OH) is created when these holes react with water molecules. The hydroxyl radical's potent oxidizing ability is what causes organic dyes to break down; in this process, non-toxic byproducts are also created. Super oxide anions and the hydroxyl radical have strong oxidizing and reducing characteristics that can more effectively breakdown and mineralize organic contaminants [6]. Different operational parameters, such as dye concentration, irradiation time, catalyst morphology, dose of photocatalyst, reaction temperature, dye-containing solution pH, and light intensity, have an impact on the overall photocatalytic process. The rate of dye degradation normally increases with exposure time, but after a while it stabilizes because the dye molecules have saturated the catalyst surface. Figure (4-4) shows what happened in the sample S2, which corresponds to this study [46]. Mechanism for the heterojunction SnO_2 :CuO nanocomposite is shown in fig.(3) below:

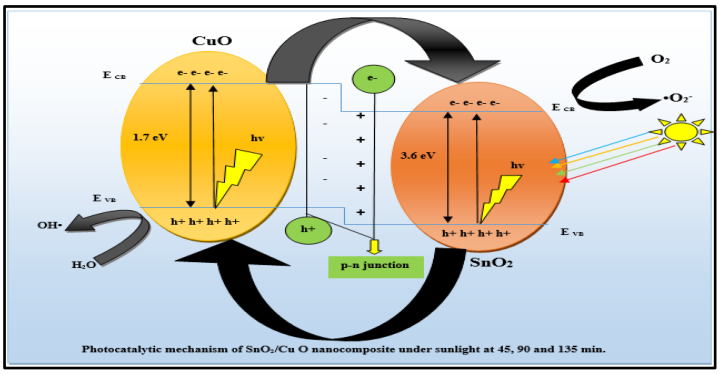

Figure 8. A schematic illustration of the photocatalytic mechanism for the heterojunction SnO_2/CuO nanoparticles

7.Conclusions

The (SnO_2:CuO) nanocomposite was created using a hydrothermal method, this method succeeded in the process of hydrothermal synthesis of nano-surface structures. The presence of both phases in the produced material is clearly demonstrated by XRD spectrum analysis, and the crystallite sizes of (SnO_2:CuO) nanostructures are calculated to fall between (45 and 54) nm, respectively. The FE-SEM picture clearly shows the creation of a morphology that is clustered, homogenous, and clearly semi-spherical, branch cauliflowers and almost spherical clusters. The absorption spectra of (SnO_2:CuO) in all the conditions mentioned show that the absorbance increases with increasing thickness layer. The thickness has a role in the energy gap, which, when the thickness layer rises, Eg falls from (2.05 into 1.98) eV. Using MB as a model pollutant, it's found that depicts the time-dependent photodegradation of methylene blue, which exhibits an increase in deterioration when exposed to sunlight. Been taken advantage sunlight to degrade emerging pollutants in water and wastewater treatment, thus preserving the environment with the SnO_2:CuO nanocomposite.

8. Reference

[1] Kaviyarasu, K., Devarajan, P. A., Xavier, S. S. J., Thomas, S. A., & Selvakumar, S. (2012). One pot synthesis and characterization of cesium doped SnO2 nanocrystals via a hydrothermal process. *Journal of Materials Science & Technology*, *28*(1), 15-20.

[2] Perumal, V., Inmozhi, C., Uthrakumar, R., Robert, R., Chandrasekar, M., Mohamed, S. B., ... & Kaviyarasu, K. (2022). Enhancing the photocatalytic performance of surface-Treated SnO2 hierarchical nanorods against methylene blue dye under solar irradiation and biological degradation. *Environmental Research*, *209*, 112821.

[3] Kasinathan, K., Kennedy, J., Elayaperumal, M., Henini, M., & Malik, M. (2016). Photodegradation of organic pollutants RhB dye using UV simulated sunlight on ceria based TiO2 nanomaterials for antibacterial applications. *Scientific reports*, *6*(1), 38064.

[4] Chandrasekar, M., Panimalar, S., Uthrakumar, R., Kumar, M., Saravanan, M. R., Gobi, G., ... & Kaviyarasu, K. (2021). Preparation and characterization studies of pure and Li+ doped ZnO nanoparticles for optoelectronic applications. *Materials Today: Proceedings*, *36*, 228-231.

[5] Arularasu, M. V., Anbarasu, M., Poovaragan, S., Sundaram, R., Kanimozhi, K., Magdalane, C. M., ... & Maaza, M. (2018). Structural, optical, morphological and microbial studies on SnO2 nanoparticles prepared by co-precipitation method. *Journal of nanoscience and nanotechnology*, *18*(5), 3511-3517.

[6] George, A., Raj, D. M. A., Venci, X., Raj, A. D., Irudayaraj, A. A., Josephine, R. L., ... & Kaviyarasu, K. (2022). Photocatalytic effect of CuO nanoparticles flower-like 3D nanostructures under visible light irradiation with the degradation of methylene blue (MB) dye for environmental application. *Environmental Research*, *203*, 111880.

[7] 7. Geetha, N., Sivaranjani, S., Ayeshamariam, A., Siva Bharathy, M., Nivetha, S., Kaviyarasu, K., & Jayachandran, M. (2018). High performance photo-catalyst based on nanosized ZnO–TiO2 nanoplatelets for removal of RhB under visible light irradiation. *Journal of Advanced Microscopy Research*, *13*(1), 12-19.

[8] Raja, A., Selvakumar, K., Rajasekaran, P., Arunpandian, M., Ashokkumar, S., Kaviyarasu, K., ... & Swaminathan, M. (2019). Visible active reduced graphene oxide loaded titania for photodecomposition of ciprofloxacin and its antibacterial activity. *Colloids and Surfaces A: Physicochemical and Engineering Aspects*, *564*, 23-30.

[9] Perumal, V., Sabarinathan, A., Chandrasekar, M., Subash, M., Inmozhi, C., Uthrakumar, R., ... & Kaviyarasu, K. (2022). Hierarchical nanorods of graphene oxide decorated SnO2 with high photocatalytic performance for energy conversion applications. *Fuel*, *324*, 124599.

[10] Manjula, N., Kaviyarasu, K., Ayeshamariam, A., Selvan, G., Diallo, A., Ramalingam, G., ... & Jayachandran, M. (2018). Structural, morphological and methanol sensing properties of jet nebulizer spray pyrolysis effect of TiO2 doped SnO2 thin film for removal of heavy metal ions. *Journal of Nanoelectronics and Optoelectronics*, *13*(10), 1543-1551.

[11] Amanulla, A. M., Magdalane, C. M., Saranya, S., Sundaram, R., & Kaviyarasu, K. (2021). Selectivity, stability and reproducibility effect of CeM-CeO2 modified PIGE electrode for photoelectrochemical behaviour of energy application. *Surfaces and Interfaces*, *22*, 100835.

[12] Thirupathy, C., Lims, S. C., Sundaram, S. J., Mahmoud, A. H., & Kaviyarasu, K. (2020). Equilibrium synthesis and magnetic properties of BaFe12O19/NiFe2O4 nanocomposite prepared by co precipitation method. *Journal of King Saud University-Science*, *32*(2), 1612-1618.

[13] Alhaji, N. M. I., Nathiya, D., Kaviyarasu, K., Meshram, M., & Ayeshamariam, A. (2019). A comparative study of structural and photocatalytic mechanism of AgGaO2 nanocomposites for equilibrium and kinetics evaluation of adsorption parameters. *Surfaces and Interfaces*, *17*, 100375.

[14] Shen, S., Chen, J., Cai, L., Ren, F., & Guo, L. (2015). A strategy of engineering impurity distribution in metal oxide nanostructures for photoelectrochemical water splitting. *Journal of Materiomics*, *1*(2), 134-145.

[15] Kennedy, J., Fang, F., Futter, J., Leveneur, J., Murmu, P. P., Panin, G. N., ... & Manikandan, E. (2017). Synthesis and enhanced field emission of zinc oxide incorporated carbon nanotubes. *Diamond and Related Materials*, *71*, 79-84.

[16] Murmu, P. P., Shettigar, A., Chong, S. V., Liu, Z., Goodacre, D., Jovic, V., ... & Kennedy, J. (2021). Role of phase separation in nanocomposite indium-tin-oxide films for transparent thermoelectric applications. *Journal of Materiomics*, *7*(3), 612-620.

[17] George, A., Raj, A. D., Irudayaraj, A. A., Josephine, R. L., Venci, X., Sundaram, S. J., ... & Kaviyarasu, K. (2022). Regeneration study of MB in recycling runs over nickel vanadium oxide by solvent extraction for photocatalytic performance for wastewater treatments. *Environmental Research*, *211*, 112970.

[18] Kumar, A., Rout, L., Achary, L., Mohanty, A., Marpally, J., Chand, P. K., & Dash, P. (2016, April). Design of binary SnO2-CuO nanocomposite for efficient photocatalytic degradation of malachite green dye. In *AIP Conference Proceedings* (Vol. 1724, No. 1). AIP Publishing.

[19] Tam, K. H., Cheung, C. K., Leung, Y. H., Djurišić, A. B., Ling, C. C., Beling, C. D., ... & Ge, W. K. (2006). Defects in ZnO nanorods prepared by a hydrothermal method. *The Journal of Physical Chemistry B*, *110*(42), 20865-20871.
[20] Yang, G., & Park, S. J. (2019). Conventional and microwave hydrothermal synthesis and application of functional materials: A review. *Materials*, *12*(7), 1177.
[21] Xu, Y. J., Zhuang, Y., & Fu, X. (2010). New insight for enhanced photocatalytic activity of TiO2 by doping carbon nanotubes: a case study on degradation of benzene and methyl orange. *The Journal of Physical Chemistry C*, *114*(6), 2669-2676.
[22] Sangchay, W. (2016). The self-cleaning and photocatalytic properties of TiO2 doped with SnO2 thin films preparation by sol-gel method. *Energy Procedia*, *89*, 170-176.
[23] Said, M. I., & Othman, A. A. (2021). Structural, optical and photocatalytic properties of mesoporous CuO nanoparticles with tunable size and different morphologies. *RSC advances*, *11*(60), 37801-37813.
[24] Seo, D. H., Lee, J. S., Yun, S. D., Yang, J. H., Huh, S. C., Sung, Y. M., ... & Noh, J. P. (2022). Electrochemical Properties of Multilayered Sn/TiNi Shape-Memory-Alloy Thin-Film Electrodes for High-Performance Anodes in Li-Ion Batteries. *Materials*, *15*(7), 2665.
[25] Nwanna, E. C., Imoisili, P. E., & Jen, T. C. (2022). Green synthesis preparation and evaluation of CuO doped SnO2. *journal of materials research and technology*, *17*, 1901-1910..
[26] Piešová, M., Czán, A., Šajgalík, M., Czánová, T., & Čep, R. (2017). Experimental quantification of the austenitic phase in steels using the Average peak method of x-ray diffractometry. *Procedia engineering*, *192*, 689-694.
[27] Faisal, A. D., Aljubouri, A. A., & Khalef, W. K. (2022). Photodetector fabrication based on heterojunction of CuO/SnO2/Si nanostructures. *Bulletin of Materials Science*, *45*(2), 84.
[28] RJayaseelan, M. (2017). Synthesis and Characterization of Virgin and Ag doped CuO: SnO2 Mixed Composites. *DJ Journal of Engineering Chemistry and Fuel*, *2*(1).
[29] Leangtanom, P., et al., Highly sensitive and selective sensing of H2S gas using precipitation and impregnation-made CuO/SnO2 thick films. Nanoscale Research Letters, 2021. 16(1): p. 70.
[30] Tripathi, R. M., & Chung, S. J. (2021). Eco-friendly synthesis of SnO2-Cu nanocomposites and evaluation of their peroxidase mimetic activity. *Nanomaterials*, *11*(7), 1798.
[31] Ansari, S. A., Khan, M. M., Kalathil, S., Nisar, A., Lee, J., & Cho, M. H. (2013). Oxygen vacancy induced band gap narrowing of ZnO nanostructures by an electrochemically active biofilm. *Nanoscale*, *5*(19), 9238-9246.
[32] Joshi, S., Ippolito, S. J., & Sunkara, M. V. (2016). Convenient architectures of Cu 2 O/SnO 2 type II p–n heterojunctions and their application in visible light catalytic degradation of rhodamine B. *RSC advances*, *6*(49), 43672-43684.
[33] Farrukh, M. A., Teck, H. B., & Adnan, R. (2010). Surfactant-controlled aqueous synthesis of SnO_2 nanoparticles via the hydrothermal and conventional heating methods. *Turkish journal of Chemistry*, *34*(4), 537-550.
[34] Chandrasekar, M., et al., Synthesis and characterization studies of pure and Ni doped CuO nanoparticles by hydrothermal method. Journal of King Saud University-Science, 2022. 34(3): p. 101831.

[35] Khan, I., et al., Structural and optical properties of gel-combustion synthesized Zr doped ZnO nanoparticles. Optical Materials, 2013. 35(6): p. 1189-1193.
[36] Hussein, H.A. and K.H. Al-Mayalee, Study the Effect of Thickness on the Optical Properties of Copper Oxide Thin Films by FDTD Method. Turkish Journal of Computer and Mathematics Education (TURCOMAT), 2021. 12(12): p. 3865-3870.
[37] Dhineshbabu, N.R., R. Vettumperumal, and R. Kokila, A study of linear optical properties of ternary blends PVA/CMC/aloe vera biofilm for UV shielding. Applied Nanoscience, 2021. 11: p. 669-678.
[38] Hussein, D., M. Jaduaa, and A. Abd, Silver Nanoparticles (Ag NP s) Prepared By Laser Ablation In Ethanol. 2017. 3: p. 2458-925.
[39] Mohammed, I.M. and K.Y. Qader, Effect of Thickness on Optical Dispersion of SnO2 Thin Films. Diyala Journal For Pure Science, 2014. 10(3-part 1).
[40] Karkera, C., et al., Heterogeneity of photoluminescence properties and electronic transitions in copper oxide thin films: A thickness dependent structural and optical study. Ceramics International, 2018. 44(14): p. 16984-16991.
[41] Ghosh, M., et al., Role of ambient air on photoluminescence and electrical conductivity of assembly of ZnO nanoparticles. Journal of Applied Physics, 2011. 110(5).
[42] Wu, Z., et al., An ultrasound-assisted deposition of NiO nanoparticles on TiO2 nanotube arrays for enhanced photocatalytic activity. Journal of Materials Chemistry A, 2014. 2(22): p. 8223-8229.
[43] Perumal, V., et al., Electron-hole recombination effect of SnO2–CuO nanocomposite for improving methylene blue photocatalytic activity in wastewater treatment under visible light. Journal of King Saud University-Science, 2023. 35(1): p. 102388.
[44] Armaković, S.J., M.M. Savanović, and S. Armaković, Titanium dioxide as the most used photocatalyst for water purification: An overview. Catalysts, 2022. 13(1): p. 26.
[45] Xia, H., H. Zhang, and D. Xiao, Synthesis, characterization and photocatalytic activity of CuO-SnO2 nanocomposite oxide photocatalyst. Journal of Advanced Oxidation Technologies, 2007. 10(2): p. 405-410.
[46] Joshi, N.C., et al., Advances in Sno2-Based Nanomaterials for Photocatalysis, Supercapacitors, and Antibacterial Activities. 2022.